

Joint Mobile User Positioning and Passive Target Sensing using Optimized Sequential Beamforming

Aymen Hamrouni*, Sofie Pollin*[†], Hazem Sallouha*

* WaveCoRE, Department of Electrical Engineering (ESAT), KU Leuven, Leuven, Belgium

[†] Interuniversity Microelectronics Centre (IMEC), Leuven, Belgium

Email: {aymen.hamrouni, sofie.pollin, hazem.sallouha}@kuleuven.be

Abstract—Integrated sensing and communication (ISAC) relies on monostatic sensing (MS) and bistatic positioning (BP) to enable comprehensive environmental awareness and user localization. However, existing frameworks predominantly assume static geometries and optimize these modalities independently, neglecting user mobility and sequential information sharing. In this paper, we propose a velocity-aware sequential beamforming framework that dynamically couples MS and BP in time. We derive the Cramér-Rao bounds (CRBs) in the position domain to formulate a non-convex resource allocation problem. Instead of relying on static weighted-sum tradeoffs, we introduce a sequential Bayesian optimization strategy where MS is executed first to construct a reliable structural prior on the UE and passive targets (PTs). This covariance prior is subsequently passed to the UE to regularize the BP estimation stage. We demonstrate that optimizing a single shared beamformer globally across both phases yields superior synergistic gains compared to a two-stage greedy approach. Simulation results validate that the shared sequential design efficiently balances limited symbol resources, achieving centimeter-level positioning accuracy for both the UE and PTs, robust velocity estimation, and a significantly reduced computational runtime.

Index Terms—Bistatic positioning, monostatic sensing, user mobility, joint beamforming design.

I. INTRODUCTION

Integrated sensing and communication (ISAC) has emerged as a fundamental design paradigm for future wireless networks, unifying communication, localization, and environmental awareness within a single infrastructure [1]. By exploiting shared spectrum and hardware, ISAC enables multi-antenna systems to simultaneously support data transmission and sensing functionalities [2]. Within this framework, sensing functionalities can be broadly categorized into Monostatic Sensing (MS) and Bistatic Positioning (BP), two complementary yet intrinsically coupled modalities that are both essential for comprehensive situational awareness [3], [4]. MS utilizes the Base Station’s (BS) co-located transmit and receive arrays to analyze round-trip echoes for environmental mapping and detection of Passive Targets (PTs) [3]. In contrast, BP leverages the spatially separated link between the BS and the User Equipment (UE), where the latter processes downlink signals to estimate its own position and velocity relative to the infrastructure [4].

When MS and BP operations share a common multi-antenna transmitter infrastructure, they fundamentally serve distinct operational requirements that compete for the same resources. From the UE perspective, high-precision positioning and ve-

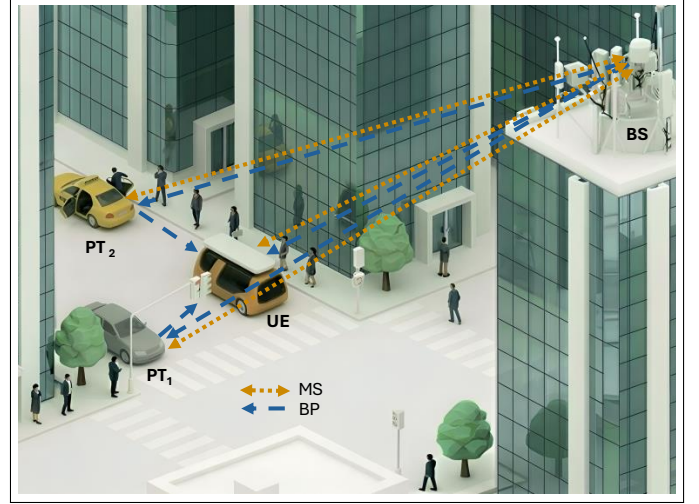


Fig. 1. Illustration of MS and BP in an urban canyon scenario. The BS simultaneously performs i) MS (orange dotted lines) to detect UE and PTs (e.g., stationary cars) and ii) BP (blue dashed lines) to enable localization and velocity estimation for the mobile UE.

locity estimation favor bistatic measurements that leverage the geometric diversity between spatially separated transmit and receive platforms to enhance the observability of the UE’s spatial-temporal state. Conversely, from the environment sensing perspective, PT detection and tracking favor monostatic radar operations, where the co-located transmitter and receiver enable coherent round-trip measurements. Consider an autonomous vehicle navigating a dense urban canyon. In such GPS-denied environments, bistatic measurements provide a crucial absolute, drift-free position and velocity reference [5]. These RF-based updates are essential to bound the cumulative drift inherent to onboard inertial measurement units (IMUs) within sensor fusion algorithms [6]. By anchoring the relative sensors, the vehicle maintains the stringent Position Error Bounds (PEB) and Velocity Error Bounds (VEB) required for safe, autonomous trajectory planning. Simultaneously, the serving Base Station utilizes MS to scan the surrounding environment to detect PTs including static objects and dynamic obstacles like pedestrians or legacy vehicles.

Fundamental spatial and time-frequency tradeoffs have been thoroughly analyzed for conventional monostatic configurations [7]. However, to overcome the limited coverage, severe path-loss scaling, and self-interference geometric con-

straints, the research community has increasingly shifted toward bistatic and multi-static deployments. For instance, Bauhofer et al. [8] proposed fusion techniques for processing information from multiple spatially separated sensing nodes to enable robust multi-target localization. Similarly, cooperative ISAC frameworks utilizing multiple base stations have demonstrated significant enhancements in PT localization [9]. Advanced multi-static architectures have been developed to improve target localization accuracy under both Line-of-Sight (LoS) and Non-Line-of-Sight (NLoS) conditions [10].

Despite these advancements in spatial observability, only recently have attempts been made to characterize these joint tradeoffs when MS and BP are jointly executed from a shared infrastructure. In these recent attempts, Cramér-Rao bound (CRB) plays a central role. The CRB enables a principled quantification of sensing and positioning accuracy in terms of transmit covariance, capturing the spatial power allocation and beamforming strategy, and array geometry, which determines the system’s spatial resolution and parameter identifiability. Among the few works addressing this, Ge et al. [11] explored fusion at the filtering stage, proposing an extended Kalman-Poisson multi-Bernoulli sequential filter to integrate maps from both monostatic and bistatic sensing modalities in 5G mmWave scenarios. Zhang et al. [12] recently investigated the performance tradeoff between BP and MS within a MIMO-OFDM system, proposing a multi-objective optimization framework based on a weighted-sum CRB to design optimal spatial beamformers. Nevertheless, existing work predominantly assumes static scenarios, neglecting the inherent mobility of practical wireless systems. In reality, UE exhibits non-negligible velocities over the sensing interval. Ignoring this mobility not only compromises model realism but also discards the valuable information embedded in Doppler shifts, which can significantly enhance both positioning and sensing performance. Furthermore, such joint operations create a fundamental resource allocation dilemma: MS demands radar-centric beamforming patterns that maximize the illumination of uncooperative environmental scatterers, whereas BP requires beamforming strategies that guarantee robust signal reception at the mobile vehicle. MS and BP directly compete for finite symbol resources within a fixed coherence interval. To the best of our knowledge, the joint BP and MS with mobile user scenarios, along with the corresponding beamforming design problem, are open research questions.

In this paper, we propose a joint MS and BP sensing framework that explicitly models UE mobility and exploits the information coupling between both sensing modalities. Unlike existing static approaches, we develop a velocity-aware, sequential beamforming design that dynamically balances positioning and environmental sensing over time. Our main contributions are summarized as follows:

- We derive the CRB for joint MS and BP in a practical mmWave MIMO-OFDM system under UE mobility. By extracting delay, angle, and Doppler parameters in the channel domain, we map them to 2D position and 2D velocity to formulate a non-convex beamforming opti-

TABLE I
CPI FOR UE CONSTANT-VELOCITY ASSUMPTION BY SCENARIO

Scenario	f_c (GHz)	v_U (m/s)	T_{CPI}
Pedestrian	28	5	~ 1.0 ms
Vehicle (urban)	28	30	~ 180 μ s
High-speed vehicle	28	50	~ 100 μ s
UAV (mmWave)	60	50	~ 50 μ s

mization under a fixed energy budget.

- We establish a sequential strategy that executes MS first to construct a reliable prior on both the UE state and environmental PTs. This prior is then parameterized via its covariance and passed to the BP stage. This ordering is critical since standalone BP is poorly conditioned for PT estimation due to limited geometric diversity and nuisance parameters (e.g., clock bias). However, injecting the MS-derived covariance regularizes the problem, enabling the UE to jointly sense the PTs and refine its own position.
- We introduce an adaptive temporal allocation policy that optimizes the distribution of finite symbol resources between the two stages, balancing direct measurement quality with the gains of covariance-level information sharing.

Our simulation results reveal that, within a given coherent block, optimizing separate greedy beamformers for the MS and BP fails to maximize the joint posterior information. Instead, a single shared beamformer, optimized globally across both stages achieves superior UE PEB, PTs PEB, and UE VEB. This performance gain stems from coherent coupling as shared illumination pattern simultaneously strengthens both the MS prior and the BP likelihood, whereas separate beamformers dilute energy through stage-wise reconfiguration. Furthermore, this proposed shared formulation requires significantly less computational runtime than the two-stage greedy approach by avoiding beam-switching, reducing the effective search space.

II. SYSTEM MODEL AND PROBLEM FORMULATION

A. System Setup

We consider a MIMO-OFDM setup with M subcarriers, where a BS equipped with N_B co-located transmit-receive antennas sends pilot signals over L slots at center frequency f_c to a UE with N_U antennas. The UE exploits these received pilots to determine its position and velocity in BP. In MS, the BS collects the echoes from PTs to infer their positions and from the UE to infer its position and velocity. In this configuration, each PT contributing to MS corresponds to a single multipath component in BP.

We assume the UE has a position $\mathbf{p}_U \in \mathbb{R}^2$ and moving with a constant velocity vector $\mathbf{v}_U \in \mathbb{R}^2$, where $v_U = \|\mathbf{v}_U\|$ denotes its speed magnitude, during a coherent processing interval (CPI). The K PTs reflectors are assumed to be static during CPI (e.g., roadside infrastructure, building facades, or parked vehicles) with unknown positions. Considering the BS’s positioning signals across L slots, we assume that each slot has a duration of T_{slot} and contains P OFDM pilot symbols

each of duration T_{sym} . The transmission start time of the (l, p) -th pilot symbol is $t_{l,p} = (l-1)T_{\text{slot}} + (p-1)T_{\text{sym}}$, where $l = 1, \dots, L$, $p = 1, \dots, P$.

The constant-velocity assumption holds provided that $T_{\text{CPI}} = t_{L,P} \leq T_c$, where the coherence time, T_c , is approximated from the maximum Doppler spread as [13]:

$$T_c \approx \frac{\lambda}{2v_{\text{rel}}}, \quad (1)$$

with wavelength $\lambda = c/f_c$ and relative velocity $v_{\text{rel}} = v_U$ since the BS and PTs are assumed static. Under this condition, the small-scale fading coefficients remain approximately constant over the CPI. Table I provides quantitative CPI limits for practical scenarios based on realistic carrier frequencies and UE velocities [14]. The transmit signal on the m -th subcarrier of the p -th symbol in the l -th slot is

$$\mathbf{x}_{l,p,m} = \mathbf{f}_l s_{p,m}, \quad (2)$$

where $\mathbf{f}_l \in \mathbb{C}^{N_B}$ is the beamformer used in slot l , and $s_{p,m}$ is a unit-modulus pilot on subcarrier m of symbol p . For clarity, we adopt the following notation convention: variables denoted as \hat{X} correspond to MS-related quantities, while variables denoted as \check{X} correspond to BP-related quantities.

B. Receive Signal for MS and BP

The signal collected for MS at the co-located BS receiver is denoted as [12]:

$$\hat{\mathbf{y}}_{l,p,m} = \hat{\mathbf{H}}_{l,p,m} \mathbf{x}_{l,p,m} + \hat{\mathbf{z}}_{l,p,m}, \quad (3)$$

with $\hat{\mathbf{z}}_{l,p,m} \sim \mathcal{CN}(\mathbf{0}, \sigma^2 \mathbf{I}_{N_B})$ is the AWGN at the BS and $\hat{\mathbf{H}}_{l,p,m} \in \mathbb{C}^{N_B \times N_B}$ is the round-trip BS-PTs/UE channel at subcarrier m , symbol p , and slot l , expressed as:

$$\begin{aligned} \hat{\mathbf{H}}_{l,p,m} &= \hat{\beta}_0 e^{-j2\pi m \Delta f \hat{\tau}_0} e^{j2\pi \hat{\nu}_0 t_{l,p}} \mathbf{a}_B(\theta_0) \mathbf{a}_B^H(\theta_0) \\ &+ \sum_{k=1}^K \hat{\beta}_k e^{-j2\pi m \Delta f \hat{\tau}_k} \mathbf{a}_B(\theta_k) \mathbf{a}_B^H(\theta_k), \end{aligned} \quad (4)$$

Here, K denotes the number of PTs and for path k , $\hat{\beta}_k$, $\hat{\tau}_k$, and θ_k are the complex gain, delay, and angle-of-departure (AOD), respectively. The UE is treated as a PT in MS and indexed by $k = 0$ and Doppler $\hat{\nu}_0$ exists only for LoS UE path. The noise power is $\sigma^2 = FN_0 \Delta f$, where F is the noise figure, N_0 is the single-sided noise PSD, and Δf is the subcarrier spacing. The vector $\mathbf{a}_B(\cdot) \in \mathbb{C}^{N_B}$ denotes the steering vectors at the BS.

The received signal at the UE for BP is expressed as [12]:

$$\check{\mathbf{y}}_{l,p,m} = \mathbf{W}^H \hat{\mathbf{H}}_{l,p,m} \mathbf{x}_{l,p,m} + \check{\mathbf{z}}_{l,p,m}, \quad (5)$$

where $\check{\mathbf{z}}_{l,p,m} \sim \mathcal{CN}(\mathbf{0}, \sigma^2 \mathbf{I}_{N_U})$ denotes AWGN at the UE and $\mathbf{W} \in \mathbb{C}^{N_U \times N_{\text{RF}}}$ is the analog combining matrix at the UE, with N_{RF} denoting the number of RF chains. The matrix $\hat{\mathbf{H}}_{l,p,m} \in \mathbb{C}^{N_U \times N_B}$ is the BS-UE channel at subcarrier m , symbol p , and slot l , modeled as:

$$\hat{\mathbf{H}}_{l,p,m} = \sum_{k=0}^K \hat{\beta}_k e^{-j2\pi m \Delta f \hat{\tau}_k} e^{j2\pi \hat{\nu}_k t_{l,p}} \mathbf{a}_U(\psi_k) \mathbf{a}_B^H(\theta_k), \quad (6)$$

where ψ_k denotes the angle-of-arrival (AOA) at the UE from path k and Doppler term $e^{j2\pi \hat{\nu}_k t_{l,p}}$ accounts for the phase evolution due to relative motion from all paths k . Here, the

LoS component is indexed by $k = 0$ and the vector $\mathbf{a}_U(\cdot) \in \mathbb{C}^{N_U}$ denotes the steering vectors at the UE.

C. CRB-Based Performance Metrics

The localization process in both MS and BP is modeled as a two-stage process where, in the first stage, channel-domain parameters are estimated, and in a second stage, these channel-domain parameters are mapped to position-domain parameters. For MS, we define the channel-domain parameter vector as:

$$\hat{\xi} = [\boldsymbol{\theta}^T, \hat{\boldsymbol{\tau}}^T, \hat{\boldsymbol{\nu}}^T, \hat{\boldsymbol{\beta}}_R^T, \hat{\boldsymbol{\beta}}_I^T]^T \in \mathbb{R}^{4K+5}, \quad (7)$$

where $\boldsymbol{\theta} = [\theta_0, \dots, \theta_K]^T$, $\hat{\boldsymbol{\tau}} = [\hat{\tau}_0, \dots, \hat{\tau}_K]^T$, $\hat{\boldsymbol{\nu}} = [\hat{\nu}_0, 0, \dots, 0]^T$, $\hat{\boldsymbol{\beta}}_R = [\Re\{\hat{\beta}_0\}, \dots, \Re\{\hat{\beta}_K\}]^T$, $\hat{\boldsymbol{\beta}}_I = [\Im\{\hat{\beta}_0\}, \dots, \Im\{\hat{\beta}_K\}]^T$. The MS position-domain parameters are written as:

$$\hat{\boldsymbol{\eta}} = [\mathbf{p}_U^T, \mathbf{v}_U^T, \mathbf{p}_1^T, \dots, \mathbf{p}_K^T, \hat{\boldsymbol{\beta}}_R^T, \hat{\boldsymbol{\beta}}_I^T]^T \in \mathbb{R}^{4K+6}. \quad (8)$$

The (i, j) -th element of the MS channel-domain Fisher Information Matrix (FIM), $\mathbf{I}_{\text{Chan}}(\hat{\xi})$, is given by [15]:

$$[\mathbf{I}_{\text{Chan}}(\hat{\xi})]_{i,j} = \frac{2}{\sigma^2} \sum_{l=1}^L \sum_{p=1}^P \sum_{m=1}^M \Re \left\{ \frac{\partial \hat{\mu}_{l,p,m}^H}{\partial [\hat{\xi}]_i} \frac{\partial \hat{\mu}_{l,p,m}}{\partial [\hat{\xi}]_j} \right\}, \quad (9)$$

where $\hat{\mu}_{l,p,m} = \hat{\mathbf{H}}_{l,p,m} \mathbf{x}_{l,p,m}$ is the noise-free observation in Eq. (3). The MS position-domain FIM can then be obtained as $\mathbf{I}_{\text{Pos}}(\hat{\boldsymbol{\eta}}) = \hat{\mathbf{J}}^T \mathbf{I}_{\text{Chan}}(\hat{\xi}) \hat{\mathbf{J}}$, with $\hat{\mathbf{J}}$ denoting the Jacobian matrix relating the position-domain parameters $\hat{\boldsymbol{\eta}}$ and channel-domain parameters $\hat{\xi}$. Hence, the lower bound on the estimation error variance for UE position and velocity and PTs positions is written as follows:

$$\text{CRB}_{\text{MS}}(p_U, v_U, p_k) = \text{tr}([\mathbf{I}_{\text{Pos}}(\hat{\boldsymbol{\eta}})^{-1}]_{1:2K+4, 1:2K+4}), \quad (10)$$

with $\text{tr}(\cdot)$ denoting the trace operation. For BP, we define the vector of channel-domain parameters as:

$$\check{\xi} = [\boldsymbol{\theta}^T, \boldsymbol{\psi}^T, \hat{\boldsymbol{\tau}}^T, \hat{\boldsymbol{\nu}}^T, \hat{\boldsymbol{\beta}}_R^T, \hat{\boldsymbol{\beta}}_I^T]^T \in \mathbb{R}^{6K+6}, \quad (11)$$

where $\boldsymbol{\psi} = [\psi_0, \dots, \psi_K]^T$ and $\hat{\boldsymbol{\nu}} = [\hat{\nu}_0, \dots, \hat{\nu}_K]^T$. The position-domain parameters for BP are collected as:

$$\check{\boldsymbol{\eta}} = [\mathbf{p}_U^T, \mathbf{v}_U^T, \mathbf{p}_1^T, \dots, \mathbf{p}_K^T, \Delta\varphi, \Delta t, \hat{\boldsymbol{\beta}}_R^T, \hat{\boldsymbol{\beta}}_I^T]^T \in \mathbb{R}^{4K+8}, \quad (12)$$

The parameter $\Delta\varphi$ denotes the BS orientation in the UE's local frame, and Δt is the clock bias capturing BS-UE asynchronism. Analogously to MS, the BP position-domain FIM is written as:

$$\mathbf{I}_{\text{Pos}}(\check{\boldsymbol{\eta}}) = \check{\mathbf{J}}^T \mathbf{I}_{\text{Chan}}(\check{\xi}) \check{\mathbf{J}}, \quad (13)$$

with $[\check{\mathbf{J}}]_{i,j} = \partial [\check{\xi}]_i / \partial [\check{\boldsymbol{\eta}}]_j$. The CRB for UE parameters of interests (i.e., position and velocity) estimation in BP is written as:

$$\text{CRB}_{\text{BP}}(p_U, v_U) = \text{tr}([\mathbf{I}_{\text{Pos}}(\check{\boldsymbol{\eta}})^{-1}]_{1:4, 1:4}). \quad (14)$$

D. MS-BP Trade-off Problem Formulation

To initially characterize the MS-BP tradeoff, we adopt a classical weighted-sum method for MOO problems, as in [12], which yields a weak Pareto frontier between MS and BP. The formulation can be written as:

$$\begin{aligned} \text{(P1)} \quad & \min_{\mathbf{F}} (1 - \alpha) \text{CRB}_{\text{MS}}(p_U, v_U, p_k) + \alpha \text{CRB}_{\text{BP}}(p_U, v_U) \\ & \text{s.t.} \quad \text{tr}(\mathbf{F}\mathbf{F}^H) \leq \frac{P_B}{M}, \end{aligned} \quad (15)$$

where $\mathbf{F} = [\mathbf{f}_1, \dots, \mathbf{f}_L] \in \mathbb{C}^{N_B \times L}$ is the beamformer matrix that \mathbf{F} collects the L beamformers and P_B is the BS transmit power budget. The constraint is normalized so that the total power across all M subcarriers equals P_B . $\alpha \in [0, 1]$ controls the objective trade-off between MS and BP. The problem (P1) is non-convex but can be relaxed to a convex Semi-Definite Programming (SDP) and can be solved efficiently using standard solvers such as CVX [12].

III. BAYESIAN-BASED SEQUENTIAL MS-BP DESIGN

The previous formulation (P1) considers the beamforming design of MS and BP independently through a weighted-sum objective, ignoring time resources and information sharing between the two operations. We extend the state-of-the-art MS-BP joint optimization framework to a sequential setting in which the spatial beamformers for BP and MS are jointly optimized, along with the pilot allocation ratio between MS and BP. In this setting, MS is executed first so the BS obtains prior information about the UE and PTs. Then, BP is optimized to refine the UE state and infer the PTs positions given this prior. Both the BS and UE share a common symbol resource. Let that be the total number of pilot symbols κ_{Total} in the coherence time T_c . κ_{Total} is partitioned into three distinct phases and is written as:

$$\kappa_{\text{Total}} = \kappa_{\text{MS}} + \kappa_{\text{MS-BP}} + \kappa_{\text{BP}}, \quad (16)$$

where κ_{MS} and κ_{BP} are the total active sensing/positioning symbols, and $\kappa_{\text{MS-BP}}$ represents the number of symbols needed for the BS to transmit the computed MS covariance matrix to the UE for BP via a communication control channel. We define the active MS allocation ratio ρ_{MS} as the fraction of the remaining allocable symbols dedicated to the monostatic sensing, which is given by:

$$\rho_{\text{MS}} \triangleq \frac{\kappa_{\text{MS}}}{\kappa_{\text{Total}} - \kappa_{\text{MS-BP}}}, \quad 0 \leq \rho_{\text{MS}} \leq 1. \quad (17)$$

The parameter ρ_{MS} dictates the optimal switching point between MS and BP, directly controlling the performance of MS at the BS and the amount of prior information versus the remaining resources available for the BP posterior.

While MS and BP observe the same physical parameters (i.e., UE and PTs states), their measurements are collected over the disjoint pilot slots κ_{MS} and κ_{BP} and are affected by distinct nuisance parameters (e.g., different hardware and clock biases). Let the shared position-domain parameter vector be defined as¹ $\boldsymbol{\eta}_p = [\mathbf{p}_U^T, \mathbf{v}_U^T, \mathbf{p}_1^T, \dots, \mathbf{p}_K^T]$. By marginalizing out the stage-specific nuisances via the Schur complement [16], we parameterize the FIM over the same parameter vector $\boldsymbol{\eta}_p$ and obtain the equivalent position-domain FIMs for each stage, denoted as $\dot{\mathbf{I}}_{\text{Pos}}$ and $\check{\mathbf{I}}_{\text{Pos}}$, for MS and BP, respectively. The posterior distribution via Bayes' theorem is then expressed as:

$$p(\boldsymbol{\eta}_p | \check{\mathbf{y}}, \check{\mathbf{y}}) \propto p(\check{\mathbf{y}} | \boldsymbol{\eta}_p) \underbrace{p(\boldsymbol{\eta}_p | \check{\mathbf{y}})}_{\text{MS-based Prior}}. \quad (18)$$

¹Note that the channel gain parameters $\hat{\beta}_R, \hat{\beta}_I, \hat{\beta}_R, \hat{\beta}_I$, are excluded, as their contribution to the position estimation is negligible [12]. In the 2D position and 2D velocity estimation, the BP clock offset Δ_t and orientation offset Δ_φ are likewise marginalized.

Consequently, the posterior FIM for $\boldsymbol{\eta}_p$ is then additive, representing the sum of the equivalent information derived from the MS-based prior and the BP likelihood. The resulting BP posterior FIM obtained from MS prior during ρ_{MS} and from BP phase during $1 - \rho_{\text{MS}}$ is written as:

$$\check{\mathbf{I}}_{\text{seq}}(\mathbf{F}_{\text{MS}}, \mathbf{F}_{\text{BP}}, \rho_{\text{MS}}) = \dot{\mathbf{I}}_{\text{Pos}}(\mathbf{F}_{\text{MS}}, \rho_{\text{MS}}) + \check{\mathbf{I}}_{\text{Pos}}(\mathbf{F}_{\text{BP}}, 1 - \rho_{\text{MS}}). \quad (19)$$

Here, the covariance matrix obtained from the MS stage, $\dot{\mathbf{I}}_{\text{Pos}}^{-1}$, is passed as a prior to the UE during the $\kappa_{\text{MS-BP}}$ symbols.

In practical ISAC systems, ensuring reliable localization requires that estimation errors remain below predefined safety thresholds. Motivated by this, we aim to minimize the deviation error obtained in the MS and BP sequential phases from predefined thresholds. We define the set containing the threshold of UE position and velocity and PTs positions as \mathcal{S} . For example, the threshold of the PEB for UE in the MS phase is denoted as $\gamma_{p_U}^{\text{MS}} \in \mathcal{S}$.

A least-squares (LS) optimization problem can then be formulated as:

$$(P2) \quad \min_{\mathbf{F}_{\text{MS}}, \mathbf{F}_{\text{BP}}, \rho_{\text{MS}}} \mathcal{L}(\check{\mathbf{I}}_{\text{seq}}(\mathbf{F}_{\text{MS}}, \mathbf{F}_{\text{BP}}, \rho_{\text{MS}})^{-1}, \mathcal{S})$$

$$\text{s.t.} \quad \text{tr}(\mathbf{F}_{\text{MS}} \mathbf{F}_{\text{MS}}^H) \leq \frac{P_B}{M}, \quad (20)$$

$$\text{tr}(\mathbf{F}_{\text{BP}} \mathbf{F}_{\text{BP}}^H) \leq \frac{P_B}{M},$$

$$0 \leq \rho_{\text{MS}} \leq 1.$$

where $\mathcal{L}(\cdot, \cdot)$ is a weighted squared posterior cost taking into account the deviation of the extracted bounds in the sequential MS and posterior BP from their respective thresholds in \mathcal{S} . Weighting in $\mathcal{L}(\cdot, \cdot)$ could define the task priority (e.g., if emphasis is on obtaining better BP VEB and PEB, weights on the deviation of these terms with respect to their thresholds can be set higher). This problem tackles the tradeoff between allocating more BP symbols to improve BP estimation and allocating more MS symbols to build a more informative prior, which in turn improves BP. Solving (P2) jointly over all three variables would require a bilevel optimization: for each candidate \mathbf{F}_{MS} , the inner \mathbf{F}_{BP} problem must be solved conditioned on the resulting prior, which is computationally prohibitive. We therefore consider two tractable approaches.

A greedy two-stage approximation to (P2) in which the MS beamformer \mathbf{F}_{MS}^* is independently from (P1), with $\alpha = 0$ as follows:

$$\mathbf{F}_{\text{MS}}^* = \arg \min_{\mathbf{F}} \mathcal{L}_{\text{MS}}(\dot{\mathbf{I}}_{\text{Pos}}(\mathbf{F}, \rho_{\text{MS}})^{-1}, \mathcal{S}), \quad (21)$$

where $\mathcal{L}_{\text{MS}}(\cdot, \cdot)$ is the LS MS-only cost from (P1) with respect to \mathcal{S} . The beamformer \mathbf{F}_{MS}^* is then used during the symbol allocation ρ_{MS}^* to build environmental prior relative to the UE and PTs position thresholds. Then, \mathbf{F}_{BP}^* is subsequently optimized to minimize the posterior cost given the fixed prior $\dot{\mathbf{I}}_{\text{Pos}}(\mathbf{F}_{\text{MS}}^*, \rho_{\text{MS}})$. In this approach, the optimal beamformers are explicitly tailored and optimized to their respective phases. We refer to it as the *separate sequential beamformer* approach.

While this beamforming optimization approach provides spatial degrees of freedom and optimizes each beamformer for its respective phase, hardware or signaling constraints may dictate a single shared beamformer across the two phases. Moreover, and as it relies on a greedy two-stage procedure

TABLE II
SYSTEM, CHANNEL, AND SIMULATION PARAMETERS

Parameter	Symbol	Value
<i>System and Signal Configuration</i>		
BS antenna elements	N_{BS}	64
UE antenna elements	N_{UE}	16
Carrier frequency	f_c	28 GHz
System bandwidth	B	120 MHz
Number of subcarriers	M	1024
BS transmit power budget	P_B	-20 dBm
Number of slots	L	16
Symbols per slot	P	100
Clock bias	Δt	1 μ s
Relative orientation offset	$\Delta \varphi$	110°
<i>Noise and Environmental Model</i>		
Noise Power Spectral Density	N_0	-173 dBm/Hz
Noise figure	F	10 dB
Path loss exponent	n	3.5
Shadow fading	σ_{shadow}	8 dB
PTs RCS (MS)	$\sigma_{RCS,k}$	10 m ²
UE RCS (MS)	$\sigma_{RCS,0}$	10 m ²
<i>Performance Thresholds</i>		
UE PEB for MS	γ_{PU}^{MS}	50 cm
UE PEB for BP	γ_{PU}^{BP}	10 cm
UE VEB for BP	γ_{vU}^{MS}	10 m/s
PTs PEB for BP	γ_{pk}^{BP}	20 cm
PTs PEB for MS	γ_{pk}^{MS}	100 cm

where \mathbf{F}_{MS}^* is first optimized for the MS cost alone in (P1), and \mathbf{F}_{BP}^* is subsequently optimized for the posterior given with fixed prior from the MS, the MS beamformer might not be the optimal beamformer to produce the best prior for downstream BP. It prioritizes MS first and minimizes the MS estimation error during ρ_{MS}^* rather than the quality of the prior it provides to the BP stage, since it is optimized under $\mathcal{L}_{MS}(\cdot, \cdot)$, not the end-to-end posterior cost $\mathcal{L}(\cdot, \cdot)$. By contrast, a single shared beamformer \mathbf{F}_{seq}^* used across both phases (i.e., $\mathbf{F}_{MS}^* = \mathbf{F}_{BP}^* = \mathbf{F}_{seq}^*$) could be optimized directly against the final posterior cost, allowing it to jointly balance the MS prior quality and BP measurement quality in a single coupled optimization. Therefore, we define the following optimization problem:

$$(P3) \quad \min_{\mathbf{F}_{seq}, \rho_{MS}} \mathcal{L}(\hat{\mathbf{I}}_{seq}(\mathbf{F}_{seq}, \rho_{MS})^{-1}, \mathcal{S})$$

$$\text{s.t.} \quad \text{tr}(\mathbf{F}_{seq} \mathbf{F}_{seq}^H) \leq \frac{P_B}{M}, \quad (22)$$

$$0 \leq \rho_{MS} \leq 1,$$

where the optimal shared beamformer \mathbf{F}_{seq}^* is shared across both phases in Eq. (19). We refer to this approach as the *shared sequential beamformer* approach.

IV. EXPERIMENTAL RESULTS

In this section, we evaluate the positioning and velocity estimation performance of the sequential MS-BP configuration. Unless stated otherwise, all results are obtained for the parameters mentioned in Table II. The channel-domain FIMs for BP and MS are computed using the Slepian-Bangs formula [15] and mapped to the position-velocity domain via the corresponding Jacobians. The FIM of the channel parameters follows the standard diagonal assumption with no coupling

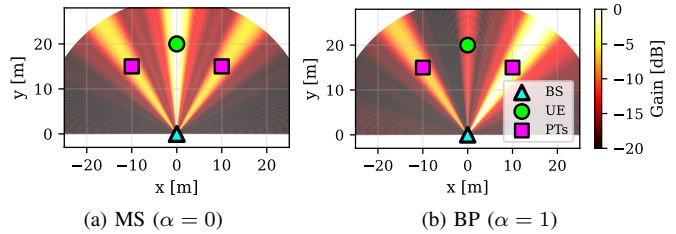


Fig. 2. Beamforming design for MS and BP. The UE and PTs are placed symmetrically at equal distances to isolate distance-dependent path-loss disparities, focusing on beamforming for MS and BP.

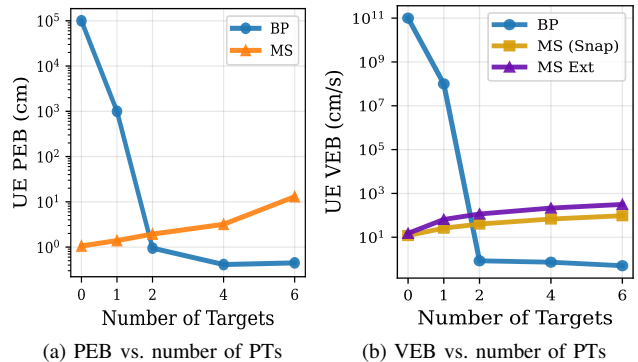


Fig. 3. PEB (log-scale) vs. number of PTs and VEB (log-scale) vs. number of PTs for BP, Snapshot MS, and Extended MS.

between delay, angle, Doppler, and channel gain estimates across different propagation paths [17]. This approximation is justified under large array apertures and high signal bandwidth conditions, where angular and temporal resolution effectively decorrelate the parameter estimation errors.

A. Beamforming Analysis

To fundamentally understand the underlying spatial allocation strategies of the two MS and BP modalities, Fig. 2 visualizes the optimized spatial beam patterns for pure MS, $\alpha = 0$, and pure BP, $\alpha = 1$. To isolate the inherent estimation requirements of each modality from path-loss biases, the simulation geometry is deliberately constructed symmetrically. As observed in Fig. 2a, the MS optimization allocates spatial energy directly toward both the PTs and the UE with more focus on the UE. This asymmetric power distribution in MS is driven by the UE velocity estimation, which relies entirely on the Doppler shift observed from the direct LoS echo. Conversely, Fig. 2b demonstrates a radically different spatial strategy for BP. The UE receives substantially lower LoS illumination energy, with the PTs on the right receiving higher energy compared to the MSs case. This occurs because FIM for BP position and velocity estimation derives critical information not only from the LoS but also from the rich signatures of the NLoS multipath components reflected off the PTs. Illuminating these PTs provides the geometric diversity required to resolve the full position and velocity. Furthermore, the highest beamforming gain is directed specifically toward the rightmost PT, due to the UE antenna array's right-tilted orientation as included in Table. II, thereby maximizing the

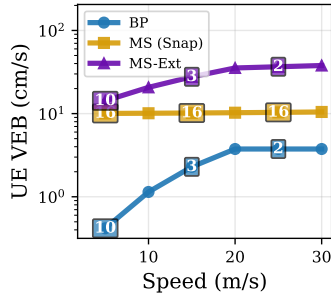


Fig. 4. VEB (log-scale) vs. speed for BP, Snapshot MS, and Extended MS with 4 PTs. The numbers represent the number of effective slots $L_{\text{eff}} \leq L$ of observation of the UE.

receivable NLoS signal power and the overall spatial-temporal information gain at the UE.

B. UE Position and Velocity Estimation Study

All the following simulations are Monte Carlo simulations with 200 independent channel realizations, including random positions of UE and PTs, to ensure statistically reliable estimates of PEB and VEB. The UE and PTs are generated to be within [5, 100]m from the broadside of the BS.

We analyze the performance of UE velocity estimation and investigate the inherent coupling between position and velocity across the MS and BP sensing modalities. Estimating velocity via MS relies purely on the Doppler shift observed from the direct LoS echo, which only captures the radial component of the UE's motion vector. Consequently, if the UE has a non-negligible tangential velocity, the monostatic FIM becomes ill-conditioned, leading to unbounded velocity error bounds. To evaluate this limitation and compare it against our proposed BP framework, we consider two distinct velocity estimators²:

- **Snapshot MS:** In this approach, we simplify (P1) by completely removing velocity and Doppler from the estimation stage, effectively treating the UE as static within each coherence interval. Two temporally separated MS snapshots are then considered, each yielding a position estimate with its associated covariance. The velocity is subsequently inferred by finite differencing the two position estimates.
- **Extended MS:** This approach exploits Doppler measurements from two temporal instants under a constant-velocity model. Because the UE moves between observations, the Doppler shifts project the velocity onto two distinct LoS directions, enabling the joint reconstruction of both radial and tangential velocity components.

Fig.3 illustrates the evolution of the PEB and VEB with respect to the number PTs. In Fig. 3(a), the PEB for BP is initially unresolved when a single PT is present, since the system lacks sufficient geometric diversity to infer both position and synchronization parameters. Once 2 or more targets are introduced, matching the minimum dimensional

²We note that while BP estimates velocity instantaneously, both Snapshot MS and Extended MS inherently suffer from latency, as velocity can only be resolved after the second temporal observation.

requirement, the BP configuration rapidly becomes more informative and surpasses the MS performance. In contrast, the PEB of MS increases with the number of PTs, as multiple spatial beams must be steered toward different directions, reducing the energy and directivity available along LoS path to the user equipment. The same trend is reflected in Fig.3b for the VEB. Both the snapshot and extended MS estimators exhibit performance degradation with additional targets for the same reason: the transmit power and beamforming gain are increasingly distributed over non-LoS directions. The degradation is more pronounced for the extended MS case, which strongly depends on the resolvability of the tangential velocity component, particularly sensitive to the UE relative position during the second observation interval. The snapshot MS, in contrast, derives its velocity information indirectly from the position covariance, resulting in a more gradual performance loss as the number of PTs grows.

Fig. 4 analyzes velocity estimation. We plot the UE VEB versus speed for Snapshot MS, Extended MS, and BP. As the speed increases, the VEB degrades for Snapshot MS and Extended MS. This trend is explained by the reduced number of effective observation slots within a CPI as higher Doppler accelerates the phase rotation across symbols/subcarriers, which shortens the interval over which the assumed parametric model remains informative and thereby lowering the usable Fisher information. BP consistently perform better than Snapshot MS and Extended MS.

C. MS/BP Allocation and Sequential Optimization

In Fig.5, we consider different UE velocities in [5, 30](m/s) and also different numbers of PTs between 2 and 4, and we compare the full MS, full BP, the shared sequential beamformer, and the separate sequential beamformer approaches by evaluating the UE PEB, UE VEB, PTs PEB, and computation time. We can see that the shared and separate sequential beamformer approach consistently yields better performances compared to full MS and full BPs. In particular, both sequential designs achieve cm-level positioning accuracy for the UE and the PTs over the considered scenarios. Parametrizing the BP FIM via the separate and shared beamformers improves conditioning, enabling the UE estimation of PTs positions, unlike in the full BP baseline. Fig. 5 also reveals that full MS performance degrades with decreasing ρ_{MS} ratio, illustrating the fundamental tradeoff between monostatic prior quality and the posterior information available from the BP stage in the sequential designs. The optimization problems (P2) and (P3) resolve this tradeoff by determining the optimal ρ_{MS}^* that minimizes the desired bounds.

Fig. 5a, Fig. 5b, and Fig. 5c show that the shared sequential beamformer consistently outperforms the separate sequential design in both UE and PTs positioning, despite the latter having more spatial degrees of freedom. This behavior originates from the joint spatio-temporal structure imposed by the shared beamformer, which maintains a consistent illumination pattern across the MS and BP stages. Because the same beams coherently interrogate the scene over time, the

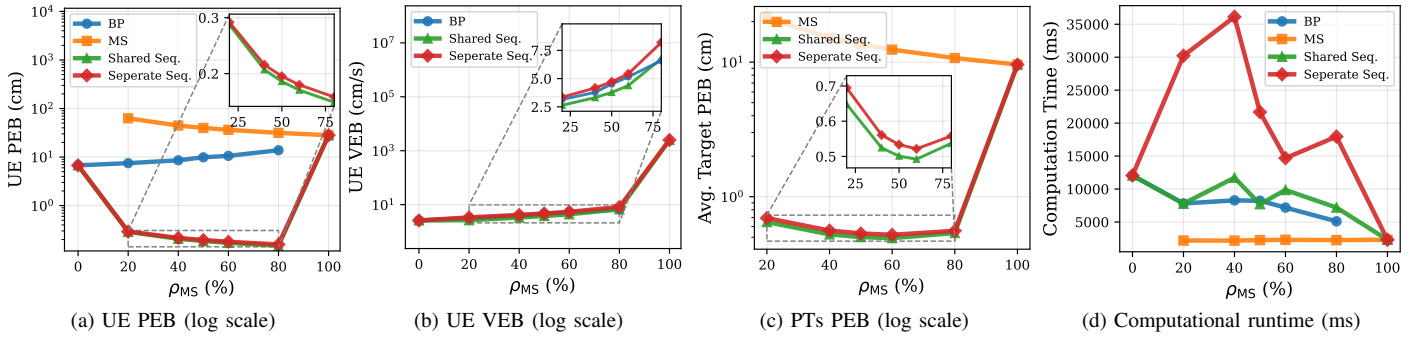


Fig. 5. Performance of full MS, full BP, shared sequential, and separate sequential beamforming designs vs. the MS symbol ratio ρ_{MS} .

Doppler and delay shifts associated with both the UE and PTs become more accurately captured, effectively enhancing parameter resolvability. Furthermore, velocity estimation relies predominantly on the BP Doppler measurement, to which the MS stage contributes only the radial component. By contrast, the separate approach commits \mathbf{F}_{MS}^* based solely on the MS cost, distributing power more broadly across directions and thus weakening the prior information passed to the BP stage for each individual node. Also, all the metrics show that MS prior dominates the lack of BP symbols.

Finally, we compare the computational running time of the different designs in Fig. 5d. The separate sequential beamformer exhibits a noticeably higher runtime than the shared counterpart due to it being implemented as a two-stage greedy optimization: it first optimizes \mathbf{F}_{MS} and then, conditioned on this choice, optimizes \mathbf{F}_{BP} over a second search space. In contrast, the shared formulation solves a single global optimization problem over a common beamformer used in both stages, which effectively reduces the dimensionality and decouples the search from stage-specific reconfiguration.

V. CONCLUSION

In this paper, we proposed a velocity-aware, sequential beamforming framework for joint monostatic sensing (MS) and bistatic positioning (BP). By executing MS first, the base station constructs a spatial-temporal prior regarding the environment and the mobile user, which is then utilized to regularize the subsequent BP estimation. Our results demonstrate that optimizing a single shared beamformer globally across both stages outperforms stage-specific greedy designs. This shared approach effectively maximizes the joint posterior information, achieving centimeter-level positioning and robust velocity estimation with reduced computational complexity. Future work will extend this framework to a dynamic time-series model, continuously adapting symbol allocation to the evolving network geometry, ultimately evolving into a multi-static online beamforming.

ACKNOWLEDGMENT

This work is supported by the EU-HORIZON-MSCA-2022-DN 6thSense project, Grant Agreement N°101119652, under the EU’s Programme for Research and Innovation.

REFERENCES

- [1] K. Wu, Z. Wang, S.-L. Chen, J. A. Zhang, and Y. J. Guo, “Isac: From human to environmental sensing,” *IEEE Journal of Selected Topics in Electromagnetics, Antennas and Propagation*, vol. 1, no. 1, 2025.
- [2] Z. Cui and S. Pollin, “Extracting the communication channel from monostatic sensing channels: From propagation to impact analysis,” *IEEE Transactions on Antennas and Propagation*, vol. 73, no. 8, 2025.
- [3] Z. Ye, F. Junaid, E. Ibrahim, R. Nilsson, and J. Van De Beek, “Monostatic sensing for passive ris localization and tracking,” *IEEE Wireless Communications Letters*, vol. 13, no. 5, pp. 1260–1264, 2024.
- [4] M. Bauhofer, M. Henninger, T. Wild, S. Ten Brink, and S. Mandelli, “Bistatic information fusion for positioning and tracking in integrated sensing and communication,” in *2025 IEEE Wireless Communications and Networking Conference (WCNC)*, 2025, pp. 1–6.
- [5] H. Sallouha, S. Saleh, S. De Bast, Z. Cui, S. Pollin, and H. Wymeersch, “On the ground and in the sky: A tutorial on radio localization in ground-air-space networks,” *IEEE Communications Surveys & Tutorials*, vol. 27, no. 1, pp. 218–258, 2025.
- [6] M. Tommingas, T. Laadung, S. Varbla, I. Mürsepp, and M. Mahtab Alam, “Uwb and gnss sensor fusion using ml-based positioning uncertainty estimation,” *IEEE Open Journal of the Communications Society*, vol. 6, pp. 2177–2189, 2025.
- [7] M. F. Keskin, M. M. Mojahedian, J. O. Lacruz, C. Marcus, O. Eriksson, A. Giorgetti, J. Widmer, and H. Wymeersch, “Fundamental trade-offs in monostatic isac: A holistic investigation toward 6g,” *IEEE Transactions on Wireless Communications*, vol. 24, no. 9, pp. 7856–7873, 2025.
- [8] M. Bauhofer *et al.*, “Multi-target localization in multi-static integrated sensing and communication deployments,” in *2023 2nd International Conference on 6G Networking (6GNet)*, 2023, pp. 1–4.
- [9] H. Liu, Y. Zhuo, S. Jin, and Z. Wang, “Multi-bs multi-target localization for isac systems,” in *2024 IEEE/CIC International Conference on Communications in China (ICCC)*, 2024, pp. 586–590.
- [10] K. Khosroshahi, P. Sehier, S. Mekki, and M. Suppa, “Localization accuracy improvement in multistatic isac with los/nlos condition using 5g nr signals,” in *2025 IEEE Wireless Communications and Networking Conference (WCNC)*, 2025, pp. 1–6.
- [11] Y. Ge, H. Kim, L. Svensson, H. Wymeersch, and S. Sun, “Integrated monostatic and bistatic mmwave sensing,” in *GLOBECOM 2023 - 2023 IEEE Global Communications Conference*, 2023, pp. 3897–3903.
- [12] Y. Zhang, H. Chen, P. Zheng, B. Ning, H. Niu, H. Wymeersch, and T. Y. Al-Naffouri, “Joint bistatic positioning and monostatic sensing: Optimized beamforming and performance tradeoff,” *IEEE Transactions on Cognitive Communications and Networking*, vol. 11, no. 5, 2025.
- [13] L. Cheng *et al.*, “Doppler spread and coherence time of rural and highway vehicle-to-vehicle channels at 5.9 ghz,” in *IEEE GLOBECOM 2008 - 2008 IEEE Global Telecommunications Conference*, 2008.
- [14] T. McKelvey and P. Dammert, “A waveform model for bistatic radar with arbitrary long coherent processing interval,” in *2025 33rd European Signal Processing Conference (EUSIPCO)*, 2025, pp. 2232–2236.
- [15] M. F. Keskin *et al.*, “Optimal spatial signal design for mmwave positioning under imperfect synchronization,” *IEEE Transactions on Vehicular Technology*, vol. 71, no. 5, 2022.
- [16] Y. Shen and M. Z. Win, “Fundamental limits of wideband localization—part i: A general framework,” *IEEE Transactions on Information Theory*, vol. 56, no. 10, pp. 4956–4980, 2010.
- [17] T. Wilding, S. Grebien, U. Mühlmann, and K. Witrisal, “Accuracy bounds for array-based positioning in dense multipath channels,” *Sensors*, vol. 18, no. 12, p. 4249, 2018.